15. The Carbon Cycle over the Past 1000 Years Inferred from the Inversion of Ice Core Data

Cathy Trudinger, Ian Enting, David Etheridge,
Roger Francey, and Peter Rayner

15.1 Introduction

Atmospheric CO_2 has increased by almost 30% since preindustrial times as a result of anthropogenic activities. The anthropogenic CO_2 perturbation sits on top of the natural variability of the carbon cycle that occurs on a range of timescales. To understand CO_2 variations over the past 1000 years, we need to consider exchanges between the atmosphere, the oceans and the terrestrial biosphere, and, in recent centuries, the anthropogenic source of CO_2 from the burning of fossil fuels. Climate is the most important driver of natural variations in exchange between the reservoirs. In the oceans, temperature and wind-speed influence CO_2 solubility, air-sea gas exchange rates, biological activity, and ocean circulation, all of which influence CO_2 fluxes. Temperature and precipitation influence photosynthesis and respiration for the terrestrial biosphere.

The anthropogenic CO_2 perturbation is due to fossil fuel burning, cement production, and changes in land use: for example, biomass burning, harvest of forests, clearing of natural forests for agriculture, and afforestation (Houghton 1995; see also Kammen and Marino 1993). The oceans and terrestrial biosphere have responded to the higher levels of CO_2 in the atmosphere by taking up some of the extra CO_2. In the case of oceans, this response is due to the partial pressure differences across the air-sea interface; for the terrestrial biosphere, it is due to the CO_2 fertilization effect (Wullschleger, Post, and King 1995). To what extent this response will continue into the future is the subject of ongoing research.

Measurements from Antarctic ice cores are an important source of CO_2 data prior to continuous high-quality direct atmospheric measurements, which began in 1958. Air trapped in bubbles in polar ice is extracted and measured to reconstruct past levels. The processes involved in storing air in the ice, which are mainly bubble trapping and diffusion through the porous firn layer, influence the trapped concentrations (see Chapter 4). They cause fractionation and smoothing of the concentration record in time relative to the actual atmospheric variations, so that high-frequency variations are not recorded in the ice. The degree of smoothing and fractionation depends on the snow accumulation rate and the depth of the firn layer and can be quantified with a numerical model of the firn processes (Schwander, Stauffer, and Sigg 1988; Trudinger et al. 1997). As Antarctica is far from most CO_2 source regions, and CO_2 is well mixed in the atmosphere on timescales of more than a year, the ice core measurements reflect global changes.

The minor stable isotope ^{13}C in CO_2 can be used to distinguish between the uptake of atmospheric CO_2 by the oceans and terrestrial biosphere due to the different degrees of isotopic fractionation associated with exchange with each reservoir. Uptake of CO_2 by plants and the oceans both discriminate against ^{13}C, but the discrimination associated with the uptake by plants is about a factor of 10 greater than that for the oceans (Keeling et al. 1989). Isotopic composition is usually expressed in the $\delta^{13}C$ notation, defined as

$$\delta^{13}C = \left(\frac{^{13}C/^{12}C_{\text{sample}}}{^{13}C/^{12}C_{\text{standard}}} - 1 \right) \times 1000 \tag{15.1}$$

in units of ‰ (permil). The more negative the $\delta^{13}C$ value, the more depleted the sample is in ^{13}C relative to ^{12}C. Preindustrially, atmospheric $\delta^{13}C$ was about -6.5‰. Present levels are below -8.0‰ and continue to decrease due to the addition of fossil fuel CO_2, which is depleted in ^{13}C. While $\delta^{13}C$ can tell us more about carbon fluxes than is possible with just CO_2 alone, there are complications.

The budget of CO_2 (in GtC yr^{-1}, where GtC is gigatonnes carbon, 1 Gt = 10^{15} g) can be expressed as

$$\begin{aligned} \frac{d}{dt}C_a &= F_f + F_{ba} - F_{ab} + F_{oa} - F_{ao} \\ &= F_f + F_b + F_o \end{aligned} \tag{15.2}$$

where C_a is the atmospheric CO_2 content, F_f is the source due to fossil fuel burning, and F_{ab}, F_{ba}, F_{ao}, and F_{oa} denote the (one-way) *gross* fluxes from the atmosphere to biosphere, biosphere to atmosphere, atmosphere to oceans, and oceans to atmosphere, respectively. The gross fluxes, of order 50–100 GtC yr^{-1}, are due to photosynthesis and respiration for the biosphere and molecular diffusion across the air-sea interface for the oceans, and they are almost balanced annually. The *net* fluxes leaving the atmosphere, today of the order of a few

GtC yr^{-1}, are given by the differences between the gross fluxes, $F_o = F_{oa} - F_{ao}$ for the oceans and $F_b = F_{ba} - F_{ab}$ for the terrestrial biosphere.

The ^{13}C budget can be expressed as

$$\begin{aligned}\frac{d}{dt}(C_a\delta_a) &= C_a\frac{d}{dt}\delta_a + \delta_a\frac{d}{dt}C_a \\ &\approx F_f(\delta_f - \delta_a) + (F_{ba} - F_{ab})\varepsilon_{ab} + F_{ba}(\delta_a^b - \delta_a) \\ &+ (F_{oa} - F_{ao})\varepsilon_{ao} + F_{oa}(\delta_a^o - \delta_a)\end{aligned} \tag{15.3}$$

(Tans, Berry, and Keeling 1993), where ε_{ij} (in permil) is the isotopic shift that occurs for a flux from reservoir i to reservoir j, and δ_a^b and δ_a^o are the isotopic ratios that the atmosphere would have if it were in isotopic equilibrium with the terrestrial biosphere and ocean, respectively. The addition of ^{13}C-depleted anthropogenic CO_2 to the atmosphere disturbs the isotopic equilibrium with the oceans and terrestrial reservoirs. The gross CO_2 fluxes reduce this disequilibrium. Terms in the atmospheric ^{13}C budget describing this effect, F_{ba} $(\delta_a^b - \delta_a)$ and F_{oa} $(\delta_a^o - \delta_a)$, are often referred to as *isofluxes* (isotopic disequilibrium fluxes). The degree of isotopic disequilibrium between the reservoirs is difficult to measure but can be modeled. Other processes can also disturb the isotopic equilibrium between the reservoirs. For example, isotopic fractionation can vary with sea-surface temperature (Heimann and Keeling 1989) or in response to water stress on plant stomata (Randerson et al. 2002). These second-order effects are quite uncertain on the global average, particularly on decadal timescales, and have generally been neglected. They will also be neglected here, but they are an aspect of ^{13}C interpretation that certainly needs further investigation.

We will use a simple box model to investigate an ice core record of CO_2 and $\delta^{13}C$ from Law Dome in Antarctica. Three modeling approaches have traditionally been used to study variations in CO_2 over recent centuries. The first is a *forward* calculation, where the model determines variations in CO_2 and $\delta^{13}C$ due to specified fluxes. The other two methods, the *single deconvolution* and *double deconvolution*, are inverse methods, and as such they deduce fluxes that are required to match the changes measured in the ice core record. In a single deconvolution, anthropogenic inputs are specified, CO_2 uptake by the ocean calculated, and terrestrial uptake deduced to match the observed variations in CO_2. In a double deconvolution, the anthropogenic fluxes are specified, and the net ocean and terrestrial fluxes determined simultaneously to match both CO_2 and $\delta^{13}C$. All three approaches will be used here to study different aspects of the Law Dome ice core record. By using these different approaches in combination, we can compare our current, somewhat limited, knowledge of the fluxes and the processes responsible for them with what the concentration and isotope data tell us. This will help us to gain a better understanding of the processes and to develop better models of the carbon cycle, which are required for predictions of future levels of CO_2. This chapter is a summary of work presented in Trudinger et al. (1999, 2002b) and Trudinger (2000).

15.2 CO_2 and $\delta^{13}C$ Over the Past 1000 Years

The Law Dome CO_2 ice core record (Fig. 15.1) from Etheridge et al. (1996) consists of ice core measurements from three cores on Law Dome, East Antarctica: DE08, DE08-2, and DSS, as well as firn measurements from DE08-2. The three cores were drilled using different techniques and dated independently. The snow accumulation rate at these sites is very high, giving the ice core record high time resolution and low smoothing due to the bubble trapping process. The smoothing is about 10 years for DE08 and DE08-2 and about 18 years for DSS (Trudinger 2000). The ice core record overlaps the modern CO_2 record, providing confirmation that the record represents atmospheric concentrations.

The most obvious feature in the CO_2 record is the strong increase in CO_2 since about 1800 due to the anthropogenic CO_2 source. In addition there is significant variability on a range of timescales, mainly due to the effects of climate on exchange between the atmosphere, oceans, and terrestrial biosphere. Between 1550 and 1800, CO_2 was about 6 ppm lower than it was during the

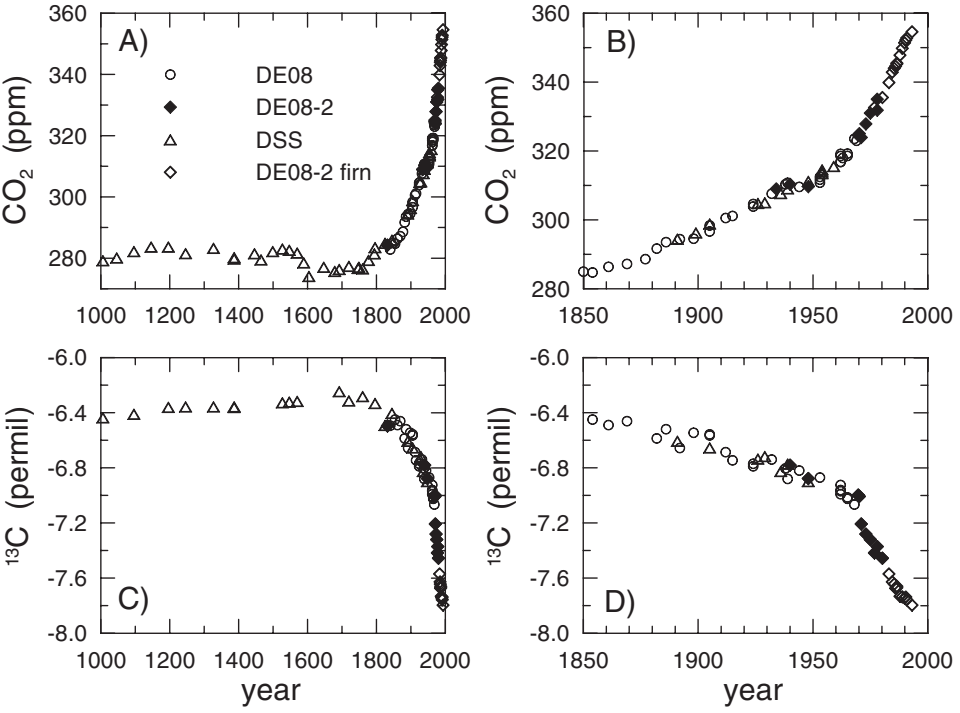

Figure 15.1. **(A)** Law Dome CO_2 ice core record over the past 1000 years (Etheridge et al. 1996); **(B)** CO_2 record, shown again since 1850; **(C)** Law Dome $\delta^{13}C$ ice core record (Francey et al. 1999); and **(D)** $\delta^{13}C$ record shown since 1850.

rest of the preindustrial period. This low CO_2 occurs during the Little Ice Age (LIA), a period of cool, dry conditions, particularly in the Northern Hemisphere (Lamb 1982; Grove 1988). The ice core shows a period of CO_2 stabilization or possibly even a decrease in CO_2 in the 1940s, at a time when the fossil fuel source was significant. The Law Dome ice core record of $\delta^{13}C$ (Francey et al. 1999) is also shown in Fig. 15.1. The record shows how $\delta^{13}C$ has decreased over the industrial period. $\delta^{13}C$ was at its highest during the LIA period, and seems not to have mirrored the flattening seen in CO_2 during the 1940s.

There is generally consistency between the Law Dome record and other ice core records of CO_2 and $\delta^{13}C$ over the past 1000 years (Neftel et al. 1985; Raynaud and Barnola 1985; Friedli et al. 1986; Pearman et al. 1986; Etheridge, Pearman, and de Silva 1988; Siegenthaler et al. 1988; Nakazawa et al. 1993; Barnola et al. 1995; Kawamura et al. 2000). However, two main differences between CO_2 records are worth noting. First, the Law Dome record does not show the increase in CO_2 in the thirteenth century that Siegenthaler et al. 1988 and Barnola et al. 1995 saw in their records. Second, the sharp decrease around 1600 seen in the Law Dome record is not seen in other records. Analytical problems associated with the earlier records may help to explain some of the differences. In addition, the Law Dome record has less smoothing in time than do the other records due to the very high accumulation rate; some differences might be expected due to the different smoothing at each site. The differences between $\delta^{13}C$ records are often larger than their measurement uncertainties. However, the Law Dome ice core record involved detailed study of systematic influences on the measurements, which seems not to have been done for the other records. Sponge records of $\delta^{13}C$ provide a method to reconstruct ocean mixed-layer $\delta^{13}C$ over the past 1000 years. The sponge records of Böhm et al. (2002) compare well with the ice core records. Due to actual differences between atmospheric and mixed-layer $\delta^{13}C$, the sponge record cannot easily be used to confirm or reject particular ice core records.

The ice core records mentioned above are all from Antarctic sites. CO_2 has also been measured in Greenland ice cores, but they show CO_2 levels that are up to 20 ppm higher than Antarctic levels (Anklin et al. 1995), with lower $\delta^{13}C$ (Francey et al. 1997). These differences are too large to be real interhemispheric gradients; the current interhemispheric gradient caused by the input of fossil fuel CO_2 (mainly into the Northern Hemisphere) is only 3 to 4 ppm. Based on measurements of CO_2, $\delta^{13}CO_2$, and CO, it is likely that the Greenland ice cores are contaminated with CO_2 derived from organic impurities (Francey et al. 1997; Haan and Raynaud 1998).

While the possibility of minor CO_2 contamination in Antarctic ice cannot be completely ruled out, Law Dome CO_2 measurements show no evidence of contamination within the analytical reproducibility of about 1 ppm. Comparison between measurements of ice core air, firn air, and atmospheric CO_2 levels, between adjacent samples of the same core with the same air age, and between CO_2 records from three Law Dome ice cores at different locations (with different accumulation and thus age-depth relations, and different chemical impurity lev-

els) show no unexplained differences (Etheridge et al. 1996; Etheridge 1999). The Law Dome ice samples were all relatively shallow (100s of meters) and thus had low bubble pressure and no evidence of clathrated air; they were also measured typically within only six years of drilling. The level of organic material in Antarctic ice is 10 to 100 times lower than in Greenland. Impurity levels are generally very low in the high accumulation snowfall of Law Dome, and CO_2 levels do not correlate with impurity levels (Etheridge 1999). Tschumi and Stauffer (2000) discussed in situ production of CO_2 due to contamination in ice. However, the Antarctic ice they studied (Byrd) was drilled many years ago and was very deep (and possibly clathrated) ice, so their results are unlikely to be applicable to Law Dome CO_2 over the past 1000 years. We therefore take the Law Dome record as an accurate representation of (smoothed) atmospheric concentrations, and we determine below what the variations in concentration and isotopic ratio imply about the net fluxes.

15.3 Modeling: Forward

The next three sections focus on interpreting features in the Law Dome record using a simple carbon cycle model (Enting and Lassey 1993; Lassey, Enting, and Trudinger 1996; Trudinger et al. 1999; Trudinger 2000). The model shown in Fig. 15.2 has 2 atmospheric boxes (troposphere and stratosphere), an ocean mixed-layer box, an Oeschger et al. (1975) diffusive deep ocean (18 layers), and a 2-box terrestrial biosphere. In addition to CO_2, the model includes the isotopes ^{13}C and ^{14}C. The model parameters are calibrated to give a good fit to measurements of CO_2 and $^{14}CO_2$.

We ran the model in forward mode, using best estimates of the CO_2 net fluxes over recent centuries, and compared the calculated CO_2 and $\delta^{13}C$ with the ice core measurements. The fluxes used were: (a) the source due to fossil fuel burning (Keeling 1997; Marland and Boden 1997); (b) the net source due to land-use change from Houghton (1995); (c) enhanced terrestrial uptake due to CO_2 fertilization (using the formulation by Allen et al. (1987) with parameters calibrated as part of the model's calibration routine); and (d) ocean uptake determined with the model.

For the calculated CO_2, $\delta^{13}C$ and the net fluxes for the forward calculation, see Fig. 15.3. The model has been tuned to match the overall industrial change in CO_2. It also matches the overall change in $\delta^{13}C$ very well ($\delta^{13}C$ was not used for calibration of the model parameters, but tuning to ^{14}C data establishes parameters that are also important for ^{13}C). The average net oceanic and terrestrial uptake in the 1980s is similar to generally accepted estimates of these quantities (Schimel et al. 1995). However, some decadal, multidecadal, and century-scale variations in the ice core record are not captured by this calculation. These variations will be the focus of the remainder of this chapter. We will look first at the LIA period.

Although the Law Dome record shows sustained low levels of CO_2 for a

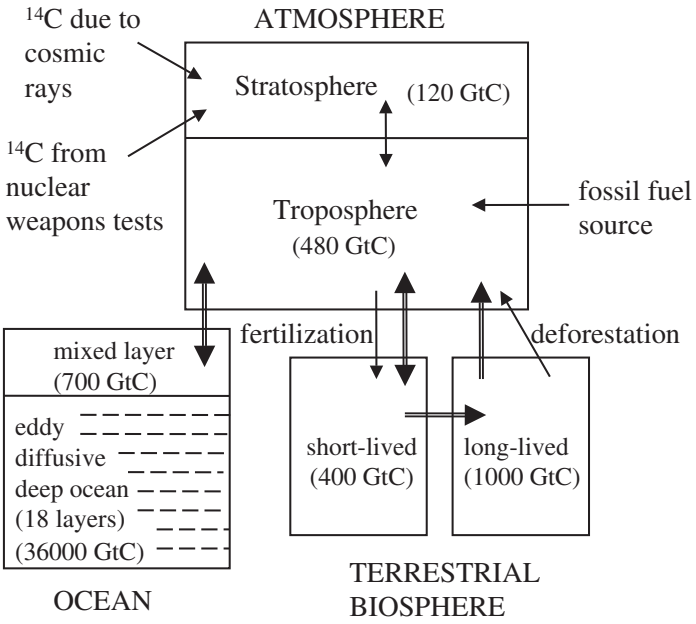

Figure 15.2. Structure of the box diffusion model, showing the fluxes between reservoirs and typical reservoir sizes.

number of centuries during the LIA period, the LIA was not a prolonged, globally synchronous climate event (Jones and Bradley 1992). Most of the well-known Northern Hemisphere climate reconstructions do show colder conditions on average over the years 1600 to 1800 compared to conditions at other times during the past 1000 years (Briffa and Osborn 2002). Although the climate reconstructions differ in their timing of the onset of cooling, the timing of the decrease in CO_2 is very clear. We will explore simple mechanisms to try to explain the high $\delta^{13}C$ and low CO_2 with temperature as a driver. The decrease in atmospheric CO_2 is unlikely to have been the primary cause of the LIA cooling (Etheridge et al. 1996). It is more likely that reduced temperatures, probably driven by volcanic and solar forcing, affected the carbon exchange between the different reservoirs, changing atmospheric CO_2 levels. The feedback of reduced CO_2 on temperature would have been small (Etheridge et al. 1996).

The forward model calculation was repeated with a hypothetical temperature record of lower temperatures during the LIA (Fig. 15.4A) and either an ocean response or a terrestrial response to this temperature variation (Trudinger et al. 1999). The hypothetical temperature record was very idealized and created so that modeled CO_2 would roughly match changes in the CO_2 ice core record. The ocean response included temperature dependence of the ocean buffer factor (Revelle and Suess 1957) and isotopic fractionation (Heimann and Keeling 1989),

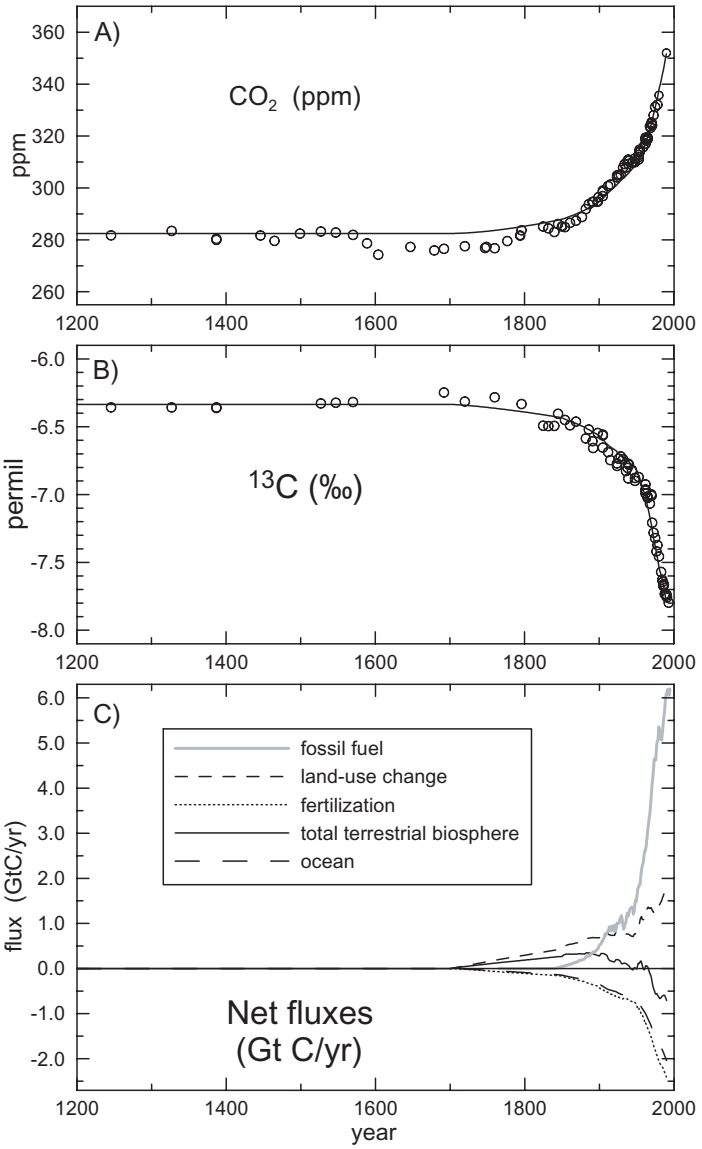

Figure 15.3. **(A)** CO_2 and **(B)** $\delta^{13}C$ calculated with the fluxes in **(C)** run forward in the carbon cycle model.

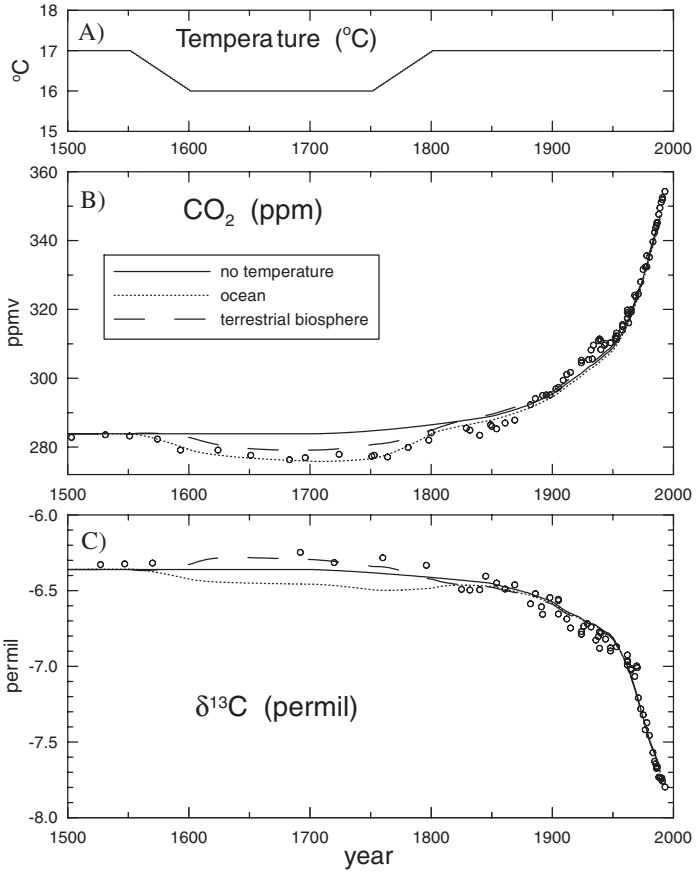

Figure 15.4. **(A)** Hypothetical temperature record used in the carbon cycle model; **(B)** Modeled CO_2; and **(C)** $\delta^{13}C$ from a forward calculation with temperature dependence of either the oceans (dotted lines) or the terrestrial biosphere (dashed lines).

and it gave a decrease in both CO_2 and $\delta^{13}C$ (dotted lines in Fig. 15.4). The terrestrial response was modeled using typical Q_{10} factors to reflect the greater sensitivity of respiration than of NPP to temperature variations (Q_{10} is the factor by which a CO_2 flux increases per 10°C of warming) (Harvey 1989). The terrestrial response to the lower temperature was a decrease in CO_2 and an increase in $\delta^{13}C$ (dashed lines in Fig. 15.4), similar to the changes observed. With such a simple model, the magnitude of the temperature response may be uncertain, but the sense of the changes should be reliable.

In the model, the effect of a temperature decrease on both terrestrial and oceanic exchange would be addition of the CO_2 decrease and partial cancellation of the $\delta^{13}C$ changes. A scenario consistent with the changes measured in the ice

core record is that global sea surface temperatures were not significantly different during the LIA, but that major terrestrial biomes experienced significant cooling. Many of the temperature records that show the cooling during this period are from Northern Hemisphere land sites, and information for the Southern Hemisphere is more limited. Etheridge et al. (1998) measured a decrease in CH_4 through this period, and a change in the interpolar difference of CH_4, consistent with lower land temperatures reducing the extent and magnitude of CH_4 emissions from wetlands in the Northern Hemisphere.

15.4 Modeling: Single Deconvolution

Global CO_2 concentrations are known better than global CO_2 fluxes. The single deconvolution calculation uses CO_2 concentration data to infer global terrestrial fluxes, with ocean fluxes determined with an ocean model. Fig. 15.5 shows CO_2, $\delta^{13}C$ and the net ocean and terrestrial fluxes from the single deconvolution. The calculation is run from AD 1200, as that is the earliest relatively steady period in the ice core record, and the model starts at steady state.

The terrestrial flux deduced in the single deconvolution minus the Houghton (1995) land-use change flux is shown by the dotted line in Fig. 15.5 Panel C. This flux varies around zero until about 1930, after which time there is a significant terrestrial uptake. Friedlingstein et al. (1995) calculated the fertilization sink with a gridded biosphere model. The time evolution of their flux was different from that suggested by a deconvolution of ice core CO_2 data: the fertilization sink, which depends on the increase of atmospheric CO_2, was larger than the deconvolution sink up to 1950, then smaller between 1960 and 1980. They suggested that other processes, such as nitrogen deposition, climate variability, or mid-latitude forest regrowth, were required to match the atmospheric CO_2.

The $\delta^{13}C$ that was calculated in the single deconvolution matches more of the variations in the ice core $\delta^{13}C$ record than $\delta^{13}C$ calculated in the forward calculation, but it is still not an exact match. Therefore more information is available from $\delta^{13}C$ about exchange of CO_2, and this will be used in the double deconvolution in the next section.

15.5 Modeling: Double Deconvolution

The forward and single deconvolution calculations use the $\delta^{13}C$ record for validation, whereas the double deconvolution uses it directly to deduce the net fluxes. Previous double deconvolutions (Francey et al. 1995; Joos and Bruno 1998; Joos et al 1999) have used the change in CO_2 and $\delta^{13}C$ through time with the budget equations of Tans, Berry, and Keeling (1993) to solve for the net fluxes by mass balance. This requires CO_2 and $\delta^{13}C$ to be known at each time step, so smoothing splines have been used to interpolate the ice core data. How-

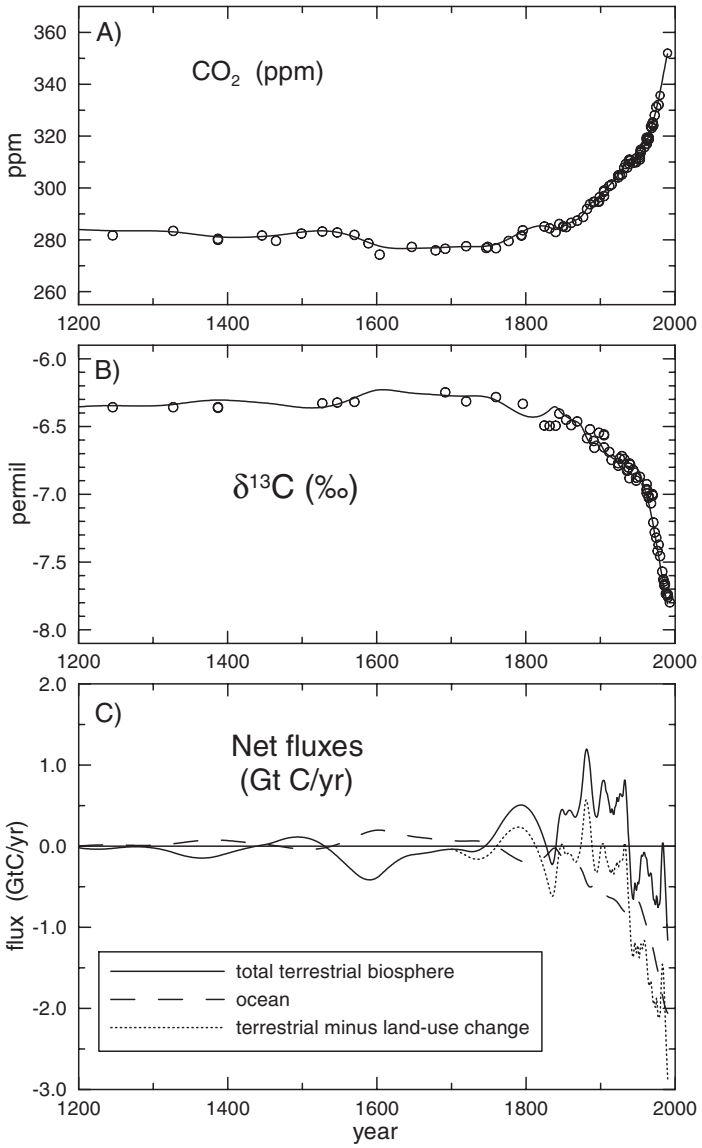

Figure 15.5. **(A)** CO_2 and **(B)** $\delta^{13}C$ and **(C)** fluxes from the single deconvolution calculation (Trudinger et al. 1999).

ever, the degree of smoothing used for the splines can have important implications for the inferred sources and their variability.

The double deconvolution described here uses the Kalman filter (Kalman 1960) to incorporate statistical analysis into the carbon cycle modeling (Trudinger 2000; Trudinger et al. 2002b). The Kalman filter is a state-space modeling technique. Data are processed sequentially to give optimal estimates of the state of the system. The carbon cycle model used with the Kalman filter is described by the budget equations of Tans, Berry, and Keeling (1993), which were given in the Introduction, with the terrestrial and oceanic components of the box diffusion model (see Fig. 15.2) used for calculation of the isofluxes. The Kalman filter double deconvolution uses the CO_2 and $\delta^{13}C$ ice core measurements, with their measurement uncertainties, to estimate the net terrestrial and oceanic fluxes.

Because the ice core record is a smoothed representation of the actual atmospheric variations, we also use a numerical model of firn diffusion and bubble trapping (Trudinger et al. 1997) to determine how concentrations are likely to vary in the firn-smoothed ice core record. Part of the variability in the ice core record is treated as signal, and part of it is treated as noise. The measurement uncertainties tell us how much can be noise, and from (off-line) calculations with the firn model we estimate how much is likely to be signal. This helps us set parameters in the Kalman filter to specify what we treat as signal versus noise (Trudinger, Enting, and Rayner 2002a). With statistical tests such as the chi-squared test (Tarantola 1987) we make sure that all of the variability in the measurements is accounted for with our statistical model.

An important feature of the calculation is that it determines the uncertainty in the estimated fluxes due to uncertainty in the measurements and evolution of the fluxes. We use a random walk model for flux evolution (Mulquiney et al. 1995). This is a weak constraint on the fluxes, and the uncertainties represent upper bounds. Uncertainty in the total net CO_2 flux and its partition into ocean and terrestrial components varies throughout the calculation, depending on the ice core data density and uncertainty, with the carbon cycle model relating CO_2, $\delta^{13}C$, the fluxes, and their uncertainties in a consistent way. For example, the uncertainty in the terrestrial flux is often lower than the uncertainty in the ocean flux, because $\delta^{13}C$ constrains the terrestrial flux better than CO_2 constrains the ocean flux with the data uncertainties we have used. In general, the flux uncertainty increases when there are long gaps in the data, which seems intuitively reasonable. Full details of the Kalman filter deconvolution calculations are given in Trudinger et al. (2002b).

Fig. 15.6 shows the results of the Kalman filter double deconvolution calculation over the past 800 years. This particular calculation has parameters chosen to give variability on century timescales (higher frequency variations such as those on the decadal timescale are treated as noise because the data density for much of the preindustrial period is insufficient to resolve them). Also shown are two temperature reconstructions: the Bradley and Jones (1993) Northern Hemisphere summer temperature anomaly record and the Mann, Bradley, and

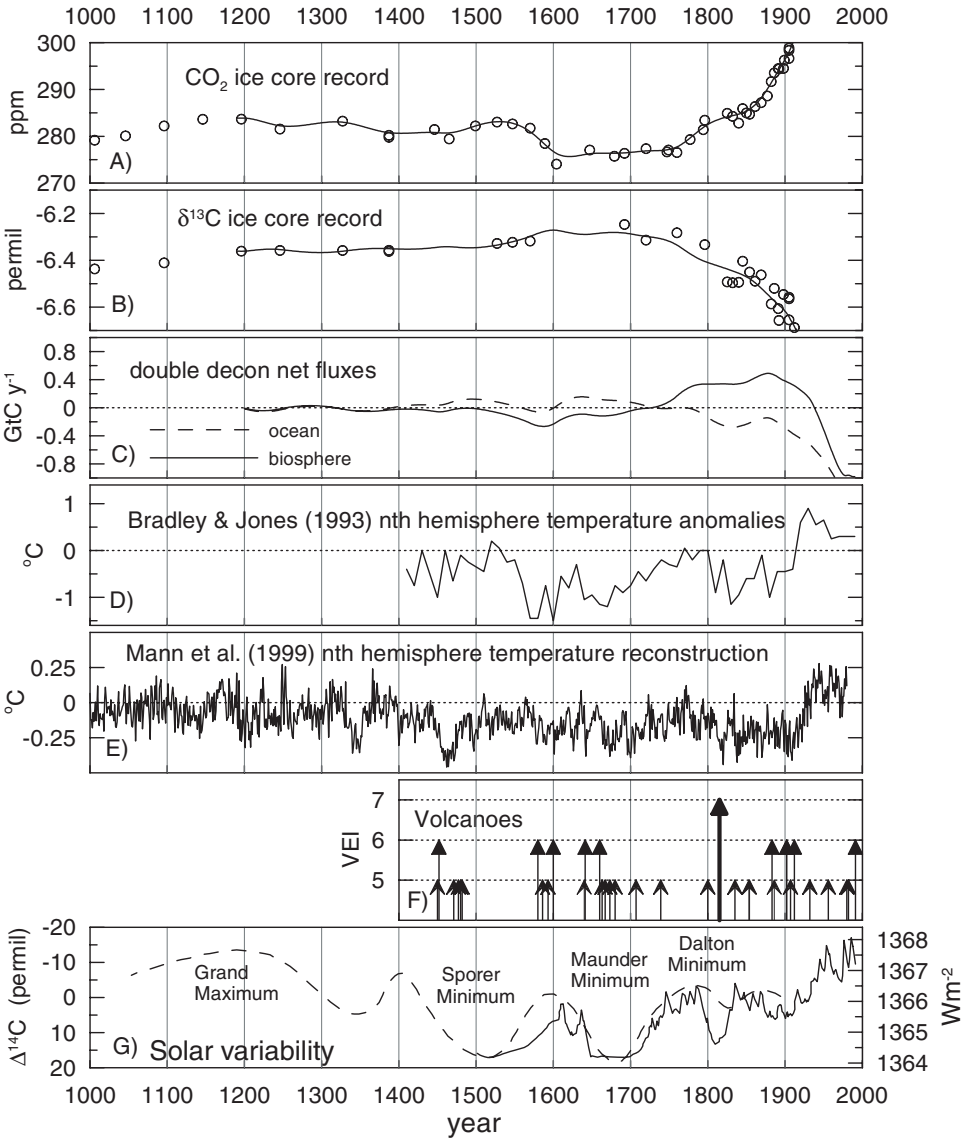

Figure 15.6. **(A)** Law Dome CO_2 measurements with the Kalman filter double deconvolution results for the century timescale (Trudinger et al. 2002b); **(B)** Law Dome $\delta^{13}C$ and the double deconvolution results; **(C)** Net fluxes from the double deconvolution; **(D)** Bradley and Jones Northern Hemisphere summer temperature anomalies; **(E)** Mann, Bradley, and Hughes (1999) Northern Hemisphere temperature reconstruction; **(F)** Volcanic Explosivity Index for the largest explosive volcanic eruptions (Briffa et al. 1998); **(G)** *solid line*, *right axis* solar irradiance reconstruction from Rind, Lean, and Healey (1999) and *dashed line*, *left axis* smoothed ^{14}C record from Eddy (1976).

Hughes (1999) temperature reconstruction. Explosive volcanic eruptions and solar forcing are believed to have an important effect on climate (Crowley 2000), and measures of their variability over the recent centuries are shown in Fig. 15.6F,G.

The Kalman filter double deconvolution and a mass balance double deconvolution by Joos et al. (1999) using the same ice core record both suggest biospheric uptake as well as an ocean source during the LIA period. Due to gaps in the data, it is not known whether $\delta^{13}C$ increased when CO_2 decreased around 1600, although the sponge record of ocean mixed-layer $\delta^{13}C$ of Böhm et al. (2002), with an almost linear increase in $\delta^{13}C$ between 1550 and 1670, suggests that it may not have increased at that time. The Kalman filter takes into account the fact that there are CO_2 but no $\delta^{13}C$ measurements around 1600, and the uncertainty in the total CO_2 flux is less than the uncertainty in the partition, as would be expected intuitively.

Biospheric uptake between about 1500 and 1750 from the Kalman filter deconvolution looks roughly like the Bradley and Jones (1993) Northern Hemisphere temperature record. The lowest temperature in the Bradley and Jones record occurs between about 1560 and 1600, when CO_2 decreased to its lowest level for the past 1000 years. The Mann, Bradley, and Hughes (1999) record has the lowest temperature for the past 1000 years at about 1460. The CO_2 measurement near 1460 is one of the lowest measurements in the record, not counting the period between 1550 and 1800 already discussed. After 1750 the biospheric flux becomes a source, and at least part (if not most) of this would have been due to land-use change.

Fig. 15.7 shows the results of the Kalman filter double deconvolution calculation since AD 1850. We have not used DSS data after 1830 in this calculation because the DSS data are inherently more smoothed in time than the DE08/DE08-2 data, and it may be inconsistent to use data with different degrees of firn smoothing without taking this into account. The estimated total flux (ocean + biosphere), minus the fluxes from the forward calculation described in Section 15.3 (i.e., land-use change, uptake due to fertilization, and modeled ocean uptake/release) is shown in Fig. 15.7C. We interpret this as the flux not already explained by the forward fluxes. Fig. 15.7D,E shows the terrestrial and oceanic fluxes, minus the terrestrial and oceanic forward fluxes. Uncertainties (1σ) from the Kalman filter are shown. This particular calculation uses a random walk parameter based on the firn model calculation and the data uncertainties given by Francey et al. (1999) for $\delta^{13}C$, and CO_2 uncertainties of 0.8 ppm.

Although Etheridge et al. (1996) suggested CO_2 uncertainties of 1.2 ppm, we choose to use the smaller CO_2 uncertainties based on the statistics of the residuals in the Kalman filter calculation. With these parameters, the Kalman filter tracks much of the decadal variation in the ice core record. This calculation pushes the ice core data to their limits, and further confirmation of features in the ice core record is needed (and planned) from new measurements. In an alternative calculation with larger data uncertainties of 1.2 ppm for CO_2 and 0.04‰ for $\delta^{13}C$, the Kalman filter essentially does not follow much of the decadal variation, as the data are thought to be too uncertain and the decadal

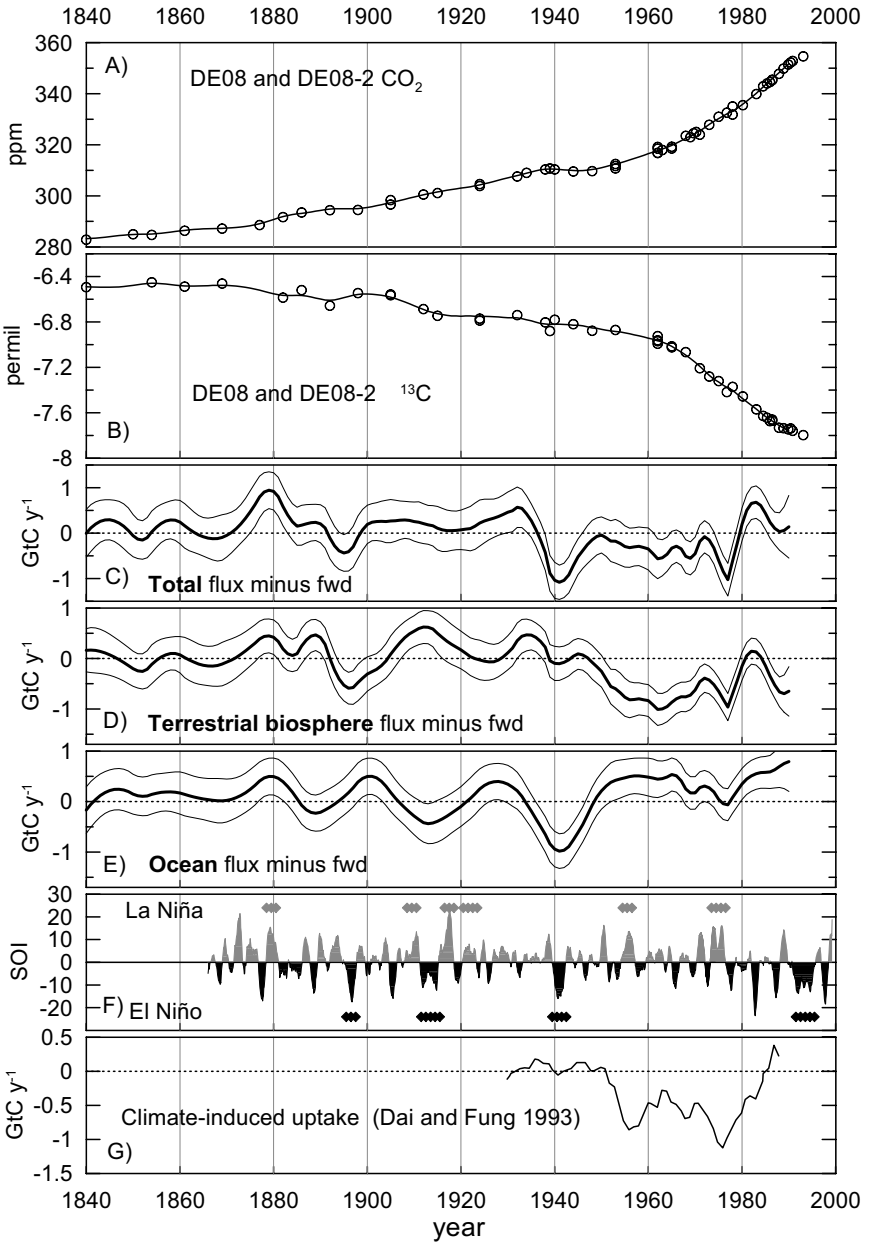

Figure 15.7. **(A)** Law Dome CO_2 measurements from 1840 with the Kalman filter double deconvolution results for the decadal timescale; **(B)** Law Dome $\delta^{13}C$ measurements from 1840 and the double deconvolution; **(C)** total CO_2 fluxes (ocean + biosphere) from the double deconvolution minus the fluxes from the forward calculation (see text) with 1σ uncertainties; **(D)** terrestrial biospheric fluxes and **(E)** oceanic fluxes, minus the forward fluxes, from the double deconvolution; **(F)** Southern Oscillation Index (11 month moving average). The diamond symbols show the extended El Niño and La Niña sequences identified by Allan and D'Arrigo (1999); and **(G)** Climate-induced biospheric CO_2 uptake from Dai and Fung (1993).

variation treated as noise rather than signal. Trudinger et al. (2002b) has more details of these calculations.

In general, the temporal structure of anomalies in the CO_2 net fluxes from our deconvolution over the industrial period is similar to that deduced by Joos et al (1999) in their mass balance double deconvolution on the same ice core record. This is not surprising given that both methods solve mass balance for the same ice core measurements. However, our deconvolution calculation suggests that natural variations in the net fluxes may be up to about 1 GtC yr^{-1} (peak-to-peak) on timescales of slightly less than a decade up to centuries, whereas the Joos et al. (1999) calculation found that natural variations were usually below ± 0.2 GtC yr^{-1} on timescales of decades to centuries. These results depend very much on the degree of smoothing used, and how variability is partitioned between signal and noise. Our calculation has assumed that many of the decadal features represent real atmospheric changes, and the firn model has shown that features such as these can survive firn smoothing. New ice core measurements will confirm which of the features are real.

Panel F of Fig. 15.7 shows the Southern Oscillation Index (11-month moving average) from http://www.dar.csiro.au/information/soi.html. The extended El Niño and La Niña events identified by Allan and D'Arrigo (1999) are indicated by the diamond symbols. Etheridge et al. (1996) noted that the persistent El Niño sequences identified by Allan and D'Arrigo (1999) around 1895 to 1898, 1911 to 1916, and 1939 to 1943 coincided with decreases in the growth rate of CO_2. We believe that the time resolution of air stored in the ice at the DE08 site (i.e., considering the smoothing by firn processes) should be sufficient to give some insight into the effect of SOI on CO_2 fluxes for the extended El Niño sequences (but not El Niño events of shorter duration). The deconvolution suggests biospheric uptake around 1895 to 1898, ocean uptake and a biospheric source around 1911 to 1916, and strong ocean uptake around 1939 to 1943. Except for the ocean uptake from 1911 to 1916, these results are all statistically significant with the data uncertainties we have used. However, the $\delta^{13}C$ variation on this timescale is sometimes defined by individual ice core measurements, which is not the ideal situation. We therefore treat these results as suggestive rather than conclusive, until the features in the ice core record can be confirmed by further measurements. The effect of ENSO on CO_2 is potentially complicated as it can involve both oceanic and terrestrial processes on a range of timescales.

We investigated the CO_2 and $\delta^{13}C$ variations corresponding with one of these extended El Niño sequences in more detail. As mentioned earlier, the CO_2 stabilization in the 1940s is a prominent feature in the Law Dome CO_2 record. The CO_2 variation is not mirrored in the $\delta^{13}C$ measurements, suggesting mainly ocean uptake. Due to the effects of firn smoothing, the real atmospheric variation would need to have been even more extreme than the ice core measurements show. We used the firn model to determine the atmospheric CO_2 variations that would have been required to leave the measured CO_2 variation trapped in the ice. This CO_2 variation was then used in the double deconvolution, with the measured $\delta^{13}C$, to see what fluxes are suggested. Large uncertainties were used

for the $\delta^{13}C$ measurements in this calculation (4 times the standard uncertainties), because firn smoothing has been accounted for in relation to CO_2 but not for $\delta^{13}C$. The calculation suggests that CO_2 uptake of up to 3 GtC yr^{-1} is required in the mid-1940s. This uptake may be up to about one-third biospheric but is mainly oceanic. If the uptake were one-third biospheric, there would have been a peak in atmospheric $\delta^{13}C$ that would not be detectable in the ice after smoothing by the firn processes. If the uptake were more than one-third biospheric, the peak in atmospheric $\delta^{13}C$ would have been too large to be consistent with the ice core measurements when smoothed. Similarly, the $\delta^{13}C$ data are not consistent with the CO_2 decrease being due to a strong decrease in the fossil fuel source at this time. This calculation suggests a cumulative uptake of up to 16 GtC between 1938 and 1951. Deconvolution of the data without taking into account the firn smoothing gives a cumulative ocean uptake of about 8 GtC between 1934 and 1949. Joos et al. (1999) found a cumulative ocean uptake of 11 GtC for this period, but their smoothing spline widens the feature compared to the amount found in our calculation.

The double deconvolution allows us to estimate terrestrial and oceanic CO_2 fluxes, but it does not immediately tell us about the processes responsible for them. That would require a process model of CO_2 exchange, and the logical next step of this work is to link the ice core inversions to a more process-based model. For now we can compare our estimated fluxes with those predicted by a process model. Fig. 15.7G shows the net terrestrial CO_2 flux due to climate variations (temperature and precipitation) calculated by Dai and Fung (1993) in a gridded model of the terrestrial biosphere. The temporal evolution and magnitude of this flux is remarkably similar to the net terrestrial flux from the double deconvolution.

15.6 Summary

In this chapter, we have investigated various features in the Law Dome CO_2 and $\delta^{13}C$ ice core record over the past 1000 years. The ice core record shows, with high precision and time resolution, the natural variability in the carbon cycle and the large anthropogenic perturbation. A simple one-dimensional carbon cycle model was used in both forward and inverse approaches to interpret the observed variations in terms of net fluxes of CO_2. As well as the standard forward and single deconvolution calculations, we used a Kalman filter double deconvolution method (Trudinger et al. 2002b). This is a new method that incorporates a rigorous statistical analysis into the carbon cycle modeling and allows quantification of the uncertainties in the inferred oceanic and terrestrial fluxes.

The main results of this work are:

- The low levels of CO_2 and high levels of $\delta^{13}C$ during the Little Ice Age period (approximately 1550 to 1800) suggest a predominantly biospheric response to reduced temperatures rather than an oceanic response.

- The double deconvolution suggests natural variability in the net CO_2 fluxes of about 1 GtC yr^{-1} on timescales of slightly less than decades up to centuries. This is greater than that suggested by a previous study and very dependent on what variation in the ice core record is considered real.
- The CO_2 flattening in the 1940s requires almost 3 GtC yr^{-1} uptake in the mid-1940s. The corresponding $\delta^{13}C$ variations suggest that most of this uptake was oceanic.
- The double deconvolution suggests variations in biospheric uptake of CO_2 between 1950 and 1980 that are very similar in both magnitude and temporal evolution to the terrestrial sink estimated by Dai and Fung (1993) using regional climate records to force globally gridded ecosystems.

The forward and inverse modeling approaches are complementary, and both are useful. The inverse approach has the advantage that global concentration is known better than global fluxes, but it has the disadvantage that the flux estimates are not linked with the processes that cause their variability. Future work will involve the use of more process-based models for flux evolution in the double deconvolution, perhaps using the Kalman filter. Confirmation of the ice core records, ideally with finer sampling density, is also needed.

References

Allan, R.J., and R.D. D'Arrigo. 1999. 'Persistent' ENSO sequences: How unusual was the 1990–1995 El Niño? *The Holocene* 9:101–18.

Allen, L.H., K.J. Boote, J.W. Jones, P.H. Jones, R.R. Valle, B. Acock, H.H. Rogers, and R.C. Dahlman. 1987. Response of vegetation to rising carbon dioxide: Photosynthesis, biomass, and seed yield of soybean. *Global Biogeochemical Cycles* 1:1–14.

Anklin, M., J.-M. Barnola, J. Schwander, B. Stauffer, and D. Raynaud. 1995. Processes affecting the CO_2 concentrations measured in Greenland ice. *Tellus* 47B:461–70.

Barnola, J.-M., M. Anklin, J. Porcheron, D. Raynaud, J. Schwander, and B. Stauffer. 1995. CO_2 evolution during the last millennium as recorded by Antarctic and Greenland ice. *Tellus* 47B:264–72.

Böhm, F., A. Haase-Schramm, A. Eisenhauer, W. Dullo, M.M. Joachimski, H. Lehnert, and J. Reitner. 2002. Evidence for preindustrial variations in the marine surface water carbonate system from coralline sponges. *Geochemistry, Geophysics, Geosystems* 3: 10.1029/2001GC000264.

Bradley, R.S., and P.D. Jones. 1993. 'Little Ice Age' summer temperature variations: Their nature and relevance to recent global warming trends. *The Holocene* 3:367–76.

Briffa, K.R., P.D. Jones, F.H. Schweingruber, and T.J. Osborn. 1998. Influence of volcanic eruptions on Northern Hemisphere summer temperature over the past 600 years. *Nature* 393:450–55.

Briffa, K.R., and T.J. Osborn. 2002. Blowing hot and cold. *Science* 295:2227–28.

Crowley, T.J. 2000. Causes of climate change over the past 1000 years. *Science* 289: 270–77.

Dai, A., and I.Y. Fung. 1993. Can climate variability contribute to the "missing" CO_2 sink. *Global Biogeochemical Cycles* 7:599–609.

Eddy, J.A. 1976. The maunder minimum. *Science* 192:1189–1202.

Enting, I.G., and K.R. Lassey. 1993. *Projections of future CO_2*. Technical paper no. 27. Aspendale, Australia: CSIRO Division Atmospheric Research.

Etheridge, D.M. 1999. Natural and anthropogenic changes in atmospheric carbon dioxide

and methane over the last 1000 years (Ph.D. thesis). Melbourne, Australia: University of Melbourne.

Etheridge, D.M., G.I. Pearman, and F. de Silva. 1988. Atmospheric trace-gas variations as revealed by air trapped in an ice core from Law Dome, Antarctica. *Annals of Glaciology* 10:28–33.

Etheridge, D.M., L.P. Steele, R.J. Francey, and R.L. Langenfelds. 1998. Atmospheric methane between 1000 AD and present: evidence for anthropogenic emissions and climate variability. *Journal of Geophysical Research* 103D:15979–93.

Etheridge, D.M., L.P. Steele, R.L. Langenfelds, R.J. Francey, J.-M. Barnola, and V.I. Morgan. 1996. Natural and anthropogenic changes in atmospheric CO_2 over the last 1000 years from air in Antarctic ice and firn. *Journal of Geophysical Research* 101D: 4115–28.

Francey, R.J., C.E. Allison, D.M. Etheridge, C.M. Trudinger, I.G. Enting, M. Leuenberger, R.L. Langenfelds, E. Michel, and L.P. Steele. 1999. A 1000-year high precision record of $\delta^{13}C$ in atmospheric CO_2. *Tellus* 51B:170–93.

Francey, R.J., E. Michel, D.M. Etheridge, C.E. Allison, M.L. Leuenberger, and D. Raynaud. 1997. The preindustrial difference in CO_2 from Antarctic and Greenland ice. In *Extended abstracts of the 5th International Carbon Dioxide Conference,* 211–12. Cairns, Australia.

Francey, R.J., P.P. Tans, C.E. Allison, I.G. Enting, J.W.C. White, and M. Trolier. 1995. Changes in oceanic and terrestrial carbon uptake since 1982. *Nature* 373:326–30.

Friedli, H., H. Loetscher, H. Oeschger, U. Siegenthaler, and B. Stauffer. 1986. Ice core record of the $^{13}C/^{12}C$ ratio of atmospheric carbon dioxide in the past two centuries. *Nature* 324:237–38.

Friedlingstein, P., I. Fung, E. Holland, J. John, G. Brasseur, D. Erickson, and D. Schimel. 1995. On the contribution of CO_2 fertilisation to the missing biospheric sink. *Global Biogeochemical Cycles* 9:541–56.

Grove, J.M. 1988. *The Little Ice Age.* New York: Methuen.

Haan, D., and D. Raynaud. 1998. Ice core record of CO variations during the last two millennia: Atmospheric implications and chemical interactions within the Greenland ice. *Tellus* 50:253–62.

Harvey, L.D.D. 1989. Effect of model structure of the response of terrestrial biosphere models to CO_2 and temperature increases. *Global Biogeochemical Cycles* 3:137–53.

Heimann, M., and C.D. Keeling. 1989. A three-dimensional model of atmospheric CO_2 transport based on observed winds: 2. Model description and simulated tracer experiments. In *Aspects of climate variability in the Pacific and the Western Americas,* Geophysical Monograph 55, ed. D. Peterson, 237–75, American Geophysical Union, Washington, D.C. (USA).

Houghton, R.A. 1995. Effects of land-use change, surface temperature and CO_2 concentration on terrestrial stores of carbon. In *Biotic feedbacks in the global climatics system: Will the warming feed the warming?* Ed. G.M. Woodwell and F.T. Mackenzie, 333–50. Oxford: Oxford University Press.

Jones, P.D., and R.S. Bradley. 1992. Climate variations over the last 500 years. In *Climate since A.D. 1500,* ed. R.S. Bradley and P.D. Jones, 649–65, New York: Routledge.

Joos, F., and M. Bruno. 1998. Long-term variability of the terrestrial and oceanic carbon sinks and the budgets of the carbon isotopes ^{13}C and ^{14}C. *Global Biogeochemical Cycles* 12:277–95.

Joos, F., R. Meyer, M. Bruno, and M. Leuenberger. 1999. The variability in the carbon sinks as reconstructed for the last 1,000 years. *Geophysical Research Letters* 26:1437–40.

Kalman, R.E. 1960. A new approach to linear filtering and prediction problems. *Journal of Basic Engineering* 82D:35–45.

Kammen, D.M., and B.D. Marino. 1993. On the origin and magnitude of pre-industrial anthropogenic CO_2 and CH_4 emissions. *Chemosphere* 26:69–86.

Kawamura, K., T. Nakazawa, T. Machida, S. Morimoto, S. Aoki, A. Ishizawa, Y. Fujii, and O. Watanabe. 2000. Variations of the carbon isotope ratio in atmospheric CO_2 over the last 250 years recorded in an ice core from H15, Antarctica. *Polar Meteorology and Glaciology* 14:47–57.

Keeling, C.D. 1997. Global historical CO_2 emissions. In *Trends: A compendium of data on global change*. Carbon Dioxide Information Analysis Center, Oak Ridge, Tennessee U.S.A.

Keeling, C.D., R.B. Bacastow, A.F. Carter, S.C. Piper, T.P. Whorf, M. Heimann, W.G. Mook, and H. Roeloffzen. 1989. A three-dimensional model of atmospheric CO_2 transport based on observed winds: 1. Analysis of observational data. In *Aspects of climate variability in the Pacific and the Western Americas*, Geophysical Monograph 55, ed. D.H. Peterson, 165–236, American Geophysical Union, Washington, D.C. (U.S.A).

Lamb, H.H. 1982. *Climate, history and the modern world*. New York: Methuen.

Lassey, K.R., I.G. Enting, and C.M. Trudinger. 1996. The Earth's radiocarbon budget: A consistent model of the global carbon and radiocarbon cycles. *Tellus* 48B:487–501.

Mann, M.E., R.S. Bradley, and M.K. Hughes. 1999. Northern hemisphere temperatures during the past millennium: Inferences, uncertainties and limitations. *Geophysical Research Letters* 26:759–62.

Marland, G., and T.A. Boden. 1997. Global, regional and national CO_2 emissions. In *Trends: A compendium of data on global change*, Carbon Dioxide Information Analysis Center, Oak Ridge, Tennessee, U.S.A.

Mulquiney, J.E., J.P. Norton, A.J. Jakeman, and J.A. Taylor. 1995. Random walks in the Kalman filter: Implications for greenhouse gas flux deductions. *Environmetrics* 6:473–78.

Nakazawa, T., T. Machida, M. Tanaka, Y. Fujii, S. Aoki, and O. Watanabe. 1993. Atmospheric CO_2 concentrations and carbon isotope ratios for the last 250 years deduced from an Antarctic ice core, H15. In *Extended abstracts of the 4th International Carbon Dioxide Conference*, 193–96. Carqueiranne, France.

Neftel, A., E. Moor, H. Oeschger, and B. Stauffer. 1985. Evidence from polar ice cores for the increase in atmospheric CO_2 in the past two centuries. *Nature* 315:45–47.

Oeschger, H., U. Siegenthaler, U. Schotterer, and A. Gugelmann. 1975. A box diffusion model to study the carbon dioxide exchange in nature. *Tellus* 27B:168–92.

Pearman, G.I., D.M. Etheridge, F. de Silva, and P.J. Fraser. 1986. Evidence of changing concentrations of atmospheric CO_2, N_2O and CH_4 from air bubbles in Antarctic ice. *Nature* 320:248–50.

Randerson, J.T., G.J. Collatz, J.E. Fessenden, A.D. Munoz, C.J. Still, J.A. Berry, I.Y. Fung, N. Suits, and A.S. Denning. 2002. A possible global covariance between terrestrial gross primary production and ^{13}C discrimination: Consequences for the atmospheric ^{13}C budget and its response to ENSO. *Global Biogeochemical Cycles* 16 doi:10.1029/2001GB001845.

Raynaud, D., and J.-M. Barnola. 1985. An Antarctic ice core reveals atmospheric CO_2 variations over the past few centuries. *Nature* 315:309–11.

Revelle, R., and H.E. Suess. 1957. Carbon dioxide exchange between the atmosphere and ocean and the question of an increase of atmospheric CO_2 during the past decades. *Tellus* 9:18–27.

Rind, D., J. Lean, and R. Healy. 1999. Simulated time-dependent climate response to solar radiative forcing since 1600. *Journal of Geophysical Research* 104:1973–90.

Schimel, D., I.G. Enting, M. Heimann, T.M.L. Wigley, D. Raynaud, D. Alves, and U. Siegenthaler. 1995. CO_2 and the carbon cycle. In *Climate change 1994: Radiative forcing of climate change and an evaluation of the IPCC emission scenarios*, 35–71. Cambridge: Cambridge University Press.

Schwander, J., B. Stauffer, and A. Sigg. 1988. Air mixing in firn and the age of the air at pore close-off. *Annals of Glaciology* 10:141–45.

Siegenthaler, U., H. Friedli, H. Loetscher, E. Moor, A. Neftel, H. Oeschger, and B. Stauffer. 1988. Stable-isotope ratios and concentrations of CO_2 in air from polar cores. *Annals of Glaciology* 10:151–56.

Tans, P.P., J.A. Berry, and R.F. Keeling. 1993. Oceanic $^{13}C/^{12}C$ observations: A new window on ocean CO_2 uptake. *Global Biogeochemical Cycles* 7:353–68.

Tarantola, A. 1987. *Inverse problem theory: Methods for data fitting and parameter estimation*. Amsterdam: Elsevier.

Trudinger, C.M. 2000. *The carbon cycle over the last 1000 years inferred from inversion of ice core data*. PhD Thesis, Monash University. [Available online at http://www.dar.csiro.au/publications/trudinger_2001a0.htm].

Trudinger, C.M., I.G. Enting, D.M. Etheridge, R.J. Francey, V.A. Levchenko, L.P. Steele, D. Raynaud, and L. Arnaud. 1997. Modeling air movement and bubble trapping in firn. *Journal of Geophysical Research* 102D:6747–63.

Trudinger, C.M., I.G. Enting, R.J. Francey, D.M. Etheridge, and P.J. Rayner. 1999. Long-term variability in the global carbon cycle inferred from a high precision CO_2 and $\delta^{13}C$ ice core record. *Tellus* 51B:233–48.

Trudinger, C.M., I.G. Enting, and P.J. Rayner. 2002a. Kalman filter analysis of ice core data: 1. Method development and testing the statistics. *Journal of Geophysical Research* 107D doi:10.1029/2001JD001111.

Trudinger, C.M., I.G. Enting, P.J. Rayner, and R.J. Francey. 2002b. Kalman filter analysis of ice core data: 2. Double deconvolution of CO_2 and $\delta^{13}C$ measurements. *Journal of Geophysical Research* 107D doi:10.1029/2001JD001112.

Tschumi, J., and B. Stauffer. 2000. Reconstructing past atmospheric CO_2 concentration based on ice-core analysis: open questions due to in situ production of CO_2 in the ice. *Journal of Glaciology* 46:45–53.

Wullschleger, S.D., W.M. Post, and A.W. King. 1995. On the potential for a CO_2 fertilisation effect in forests: Estimates of the biotic growth factors based on 58 controlled-exposure studies. In *Biotic feedbacks in the global climate system: Will the warming feed the warming?*, ed. G.M. Woodwell and F.T. Mackenzie, 85–107. Oxford University Press, U.K.